# Correlation Between Microstructure and Mechanical Properties Before and After Reversion of Metastable Austenitic Stainless Steels

GEMMA FARGAS, ANA ZAPATA, JOAN JOSEP ROA, INA SAPEZANSKAIA, and ANTONIO MATEO

Reversion treatments are a way to improve the mechanical response of metastable austenitic stainless steels by means of grain refinement. To effectively apply those treatments, the steel must be previously deformed to induce a significant amount of martensitic transformation. In this work, the effect of reversion treatments was studied on a commercial AISI 301LN grade subjected to an industrial cold rolling process, with thickness reductions not higher than 40 pct. Microstructural changes and evolution of both monotonic and cyclic mechanical properties were investigated after cold rolling and upon reversion treatments. Results revealed that the finer austenitic microstructure obtained after reversion leads to an interesting combination of properties, with strong increments in hardness and yield strength, and also fatigue limit improvement, as compared to the initial annealed condition.

DOI: 10.1007/s11661-015-3178-8


## I. INTRODUCTION

IN the past years, the demand for lightweight vehicles in order to reduce fuel consumption and also contaminant emissions has created interest in new materials to replace the classical carbon steel grades.[1] Austenitic stainless steels are presented as potential candidates for structural parts due to their excellent formability, weldability, and work hardening properties together with high corrosion resistance and high energy absorption capabilities. The main drawback is their relative low yield strength. It is well known that the addition of nitrogen is a way to improve mechanical properties by solid-solution strengthening.[2,3] Nevertheless, there is a limit for nitrogen solubility and problems with hot ductility may also appear. Strengthening by grain refining from dynamic recrystallization is another strengthening path, but severe deformations and high recrystallization temperatures are required.[4]

Among the austenitic stainless steels, those with thermodynamically metastable austenite at room temperature can be strengthening by grain refining applying thermo-mechanical processes. The procedure involves cold deformation of austenite to form strain-induced martensite followed by short annealing to revert the martensite into austenite. The amount of martensite created depends on processing parameters such as temperature and deformation rate,[5] as well as on the steel composition.[6,7] Numerous investigations have shown that ultrafine and even nanograined austenite microstructures obtained from heavy cold rolling shows an excellent combination of mechanical strength and ductility[8–10] and also excellent fatigue strength[11] together with a higher corrosion resistance as compared with cold-rolled steel.[12]

AISI 301LN austenitic stainless steel is one of the commonly used stainless steel grades for light vehicles due to its excellent combination of formability and corrosion resistance. Thanks to its capability to transform to martensite under deformation; earlier studies have demonstrated that grain refinement up to ultrafine-grained austenite is feasible by means of reversion treatments. Those studies applied severe cold rolling deformation (45 to 77 pct of thickness reduction) to achieve final improvements in strength, ductility, and fatigue behavior.[13–16] On the other hand, a recent work carried on by Huang *et al.*[17] studied the effect of annealing temperature and time on the grain size of reversed austenite from 5 to 70 pct of strain-induced martensite obtained by advanced thermo-mechanical process, where cold rolling proceeds at 273 K (0 °C). Nevertheless, some authors[18,19] have noticed that the large amount of plastic deformation necessary for grain refinement requires special procedures to be efficient and that the resulting microstructure presents large variation in morphology which causes significant scatter in mechanical properties. In this sense, the present work is focused on conventional industrial process concerning the effect of cold rolling with a thickness reduction not higher than 40 pct range where no observations or data have been published to the authors' knowledge. Correlation between microstructure and mechanical properties before and after reversion has been performed

GEMMA FARGAS, Associate Professor, ANA ZAPATA and INA SAPEZANSKAIA, Ph.D. Students, JOAN JOSEP ROA, Postdoctoral Researcher, and ANTONIO MATEO, Professor, are with the CIEFMA - Departament de Ciència del Materials i Enginyeria Metallúrgica. Universitat Politècnica de Catalunya (CIEFMA-UPC). Avda. Diagonal 647, 08028 Barcelona, Spain. Contact e-mail: gemma.fargas@upc.edu

Manuscript submitted on December 11, 2014.
Article published online September 28, 2015

regarding 10, 20, and 40 pct cold-rolled samples. Microstructural evolution was analyzed by field emission scanning electron microscopy (FESEM) and electron back-scattered diffraction (EBSD) and mechanical properties evaluated by tensile testing, hardness, and also high-cycle fatigue (HCF) tests.

## II. EXPERIMENTAL PROCESS

The experimental material was a commercial AISI 301 LN austenitic stainless steel (corresponding to standard EN 1.4318) provided by OCAS NV, Arcelor-Mittal R&D Industry Gent (Belgium). The chemical composition achieved by UV-Vis spectroscopy on a sample of the studied steel randomly selected was (in wt pct): Fe-0.03C-17.36Cr-7.18Ni-1.68Mn-0.23Mo-0.55Si-0.14N. Sheets of 1.5 mm in thickness were supplied in four different conditions: the steel named AR was subjected to cold rolling, annealing, and pickling. The cold rolling was carried out following 12 passes to achieve a thickness reduction of 75 pct. Then, the steel was annealed at 1323 K to 1353 K (1050 °C to 1080 °C) for 10 minutes to recrystallize the deformed microstructure. All oxide scales were removed by passing the strip through several consecutively mixed acid pickling baths, and then finished off with high pressure water rinsing. The three other conditions had an additional last cold rolling step performed to achieve different percentages of martensite. The thickness reductions were 10, 20, and 40 pct, for S1, S2, and S3 conditions, respectively.

Considering previous results,[20] the annealing for the complete reversion to austenite microstructure was carried out at 1023 K (750 °C) for 10 minutes. Samples subjected to this treatment are called RS1, RS2, and RS3, respectively.

Microstructural characterization was performed on the rolling plane. For optical microscopy observations, an Olympus LEXT light optical microscope was used with confocal laser scanning mode. Samples were ground and polished up to 1 $\mu$m and then electro-polished with 65 pct nitric acid solution at 12 V in order to remove martensitic transformation induced during surface preparation. Electro-etching at 1.5 V with the same solution revealed austenitic grains. 15 images of each studied steel condition were randomly selected and characterized by image analysis in order to determine the average grain size.

The phase components were identified by X-ray diffraction with Copper radiation on a Bruker D8 Advance equipment. Determination of martensite content was carried out by the method corresponding to reference intensity ratio (RIR), according to ASTM E975-03.[21] This method allows determining the mass fractions of austenite and martensite using Eq. [1]

$$\frac{X_{\alpha'}}{X_{\gamma}} = \frac{\mathrm{RIR}_{\gamma}}{\mathrm{RIR}_{\alpha'}} \times \frac{I_{\alpha',\,\mathrm{observed}}}{I_{\gamma,\,\mathrm{observed}}} \times \frac{I_{\gamma,\,\mathrm{reference}}}{I_{\alpha',\,\mathrm{reference}}}, \qquad [1]$$

where $X_{\alpha}^{'}$ and $X_{\gamma}$ are the mass fractions of $\alpha'$-martensite and $\gamma$-austenite, respectively; $\mathrm{RIR}_{\gamma}$ and $\mathrm{RIR}_{\alpha}^{'}$ are their respective RIRs; $I_{\mathrm{observed}}$ and $I_{\mathrm{reference}}$ are the observed and the reference intensities.[21]

EBSD scans were performed in a JSM-7001F FESEM equipped with Channel 5 system (HKL Technology), operating at 20 kV with samples tilted at 70 degrees. EBSD measurements were performed at 50 nm of scanning steps with beam currents of 9 nA.

Vickers hardness was measured with a MKV-HO de Akashi tester using a 0.1 kg load. Ten indents were carried out for each steel condition in order to determine the average hardness value. Nanoindentation tests were performed by a MTS Nanoindenter XP instrument equipped with continuous stiffness measurement modulus. The characterization was performed with a Berkovich tip indenter and the mechanical integrity, in terms of hardness and elastic modulus, was analyzed using the Oliver and Pharr method.[22,23] The indenter shape was carefully calibrated with a fused silica standard sample. Tests were carried out at a constant deformation rate of $5 \times 10^{-2}\ \mathrm{s}^{-1}$. The mechanical response for each specimen was assessed as the average behavior of 25 indentations, organized in a regularly spaced 5 by 5 array, at 500 nm penetration depth. A constant distance between each imprint of 50 $\mu$m was kept in order to avoid any overlapping effect.

Tensile testing was carried out at room temperature using an INSTRON 8562 computerized universal testing machine according to ASTM E 8-04,[24] at a strain rate of $4 \times 10^{-3}\ \mathrm{s}^{-1}$. Yield strength ($\sigma_{0.2}$), ultimate tensile strength ($\sigma_{\mathrm{UTS}}$), and ductility were measured for all studied steel conditions with samples were machine aligned to rolling direction. Regarding ductility, percent elongation (A pct) was computed considering the maximum elongation of the gage length divided by the original gage length (25 mm). In order to determine the amount of martensite formed during tensile tests, interrupted tests were performed at 30, 60, and 90 pct of the total elongation, and samples were extracted for X-ray diffraction determination.

Considering the tensile properties, a fatigue testing procedure was stated. It consisted of starting the tests by applying a maximum load ($\sigma_{\mathrm{max}}$) of 50 pct of the ultimate tensile strength of the corresponding steel condition and afterwards, if the specimen was able to reach $10^6$ cycles without fail, $\sigma_{\mathrm{max}}$ was increased 10 pct, and so on until fracture, following a staircase method.[25] The value of the fatigue limit was determined using the method proposed by Grove and Campean.[26]

Flat fatigue samples with hour-glass shape (Figure 1) were laser machined from the steel sheets. As in the case

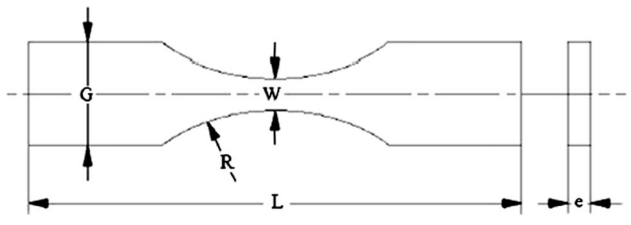


Fig. 1—Schematic representation of the fatigue specimens ($e$ = 1.5 mm, $G$ = 15 mm, $L$ = 95 mm, $R$ = 30 mm, and $W$ = 3.8 mm).

of tensile samples, load axis coincided with the rolling direction. Tests were conducted under load control in a resonant testing machine Rumul Mikroton, working at frequencies around 150 Hz. The imposed stress ratio ($R = \sigma_{min}/\sigma_{max}$) was 0.1. Before tests, samples were grinded and polished at the sides and corners up to the same roughness of the sheet surface ($R_a = 0.18 \pm 0.02$ $\mu$m) in order to avoid premature fracture due to laser cutting defects as demonstrated by the authors in a previous study.[27] It was shown that laser beam produces a significant increase of edge roughness due to overlapping of molten steel which causes a strong reduction of fatigue limit. On the other hand, microstructural changes due to laser heat were not discerned.

## III. RESULTS AND DISCUSSION

### A. *Microstructural Analysis*

Figure 2 shows the X-ray diffraction patterns of the studied samples. It can be seen that no peaks related to $\varepsilon$-martensite were detected even for the minor reduction. The fact that $\varepsilon$-martensite consists of overlapping stacking faults[17,28] implies very low intensities so that it was not identified by this technique. On the other hand, at increasing cold rolling reduction, austenite peaks gradually decreased due to the transformation to $\alpha'$-martensite, whose volume fraction is given in Table I. It has to be mentioned that martensite volume content may differ depending on the technique used,[29,30] in the case of X-ray diffraction, measurements are affected by texture.

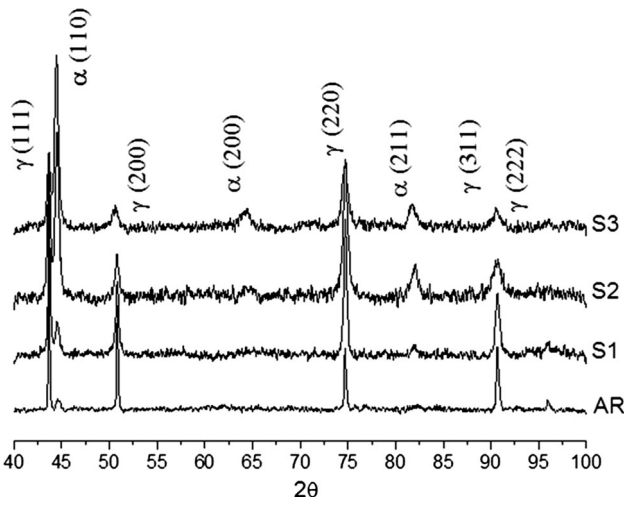


Fig. 2—X-ray diffraction patterns of the studied samples.

Stacking fault energy (SFE) plays a very important role in the deformation mechanisms. In general, a lower SFE makes dislocation cross-slip more difficult, resulting in less dislocation mobility and promoting martensitic phase transformation. Using the equation suggested by Schramm and Reed[31] (Eq. [2]), the SFE of this steel results equal to 11.2 mJ/m$^2$. SFE values for the most common austenitic stainless steels series AISI 300[32] are in the range from 9.2 to 80.3. Therefore, the studied 301LN displays a low value, and as a consequence deformation of induced martensite increases significantly with cold rolling reduction.

$$\text{SFE (mJ/m}^2) = -53 + 6.2(\text{pctNi}) + 0.7(\text{pctCr}) + 3.2(\text{pctMn}) + 9.3(\text{pctMo}) \quad [2]$$

The microstructure of the AR condition shows equiaxial austenitic grains (average grain size of $11.7 \pm 4.1$ $\mu$m) randomly oriented with twins created during annealing treatment (Figure 3). For cold-rolled samples, progressive formation of slip bands can be observed in addition to martensitic transformation (Figure 4). $\alpha'$-martensite nucleates mainly at shear bands intersections and grain boundaries for S1 samples, even though it extends rapidly across the entire grain at increasing cold rolling reductions (S2 and S3), Figure 5. There was no evidence of the presence of $\varepsilon$-martensite even for the minor cold rolling reduction. It has to be considered that the analyzed microstructures were not completely resolved by EBSD. As it is well known, highly deformed grains cannot be reliably indexed using this technique as Roa *et. al.*[33] observed for TWIP steels, and in some areas it was not possible to distinguish between slip bands in austenite and martensite.

After reversion treatments no peaks of $\alpha'$-martensite were detected, even for the samples coming from the steel condition with the highest percentage of this phase, *i.e.*, RS3. Microstructural characteristics after reversion depend on the prior percentage of cold rolling reduction.

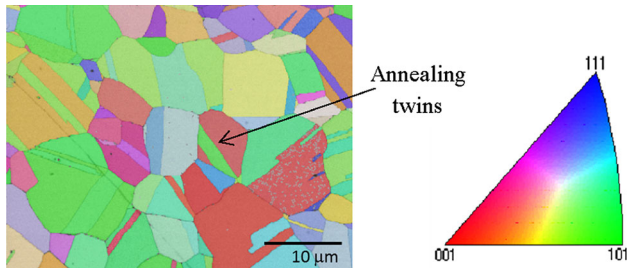


Fig. 3—EBSD orientation map of annealed sample (AR).

**Table I. Volume Fraction of Strain-Induced Martensite as a Function of Cold Rolling Reduction**

| | AR | S1 | S2 | S3 |
|---|---|---|---|---|
| Cold rolling Reduction (pct) | 0 | 10 | 20 | 40 |
| Volume fraction of martensite (pct) | 0 | 9 ± 3 | 28 ± 7 | 38 ± 5 |

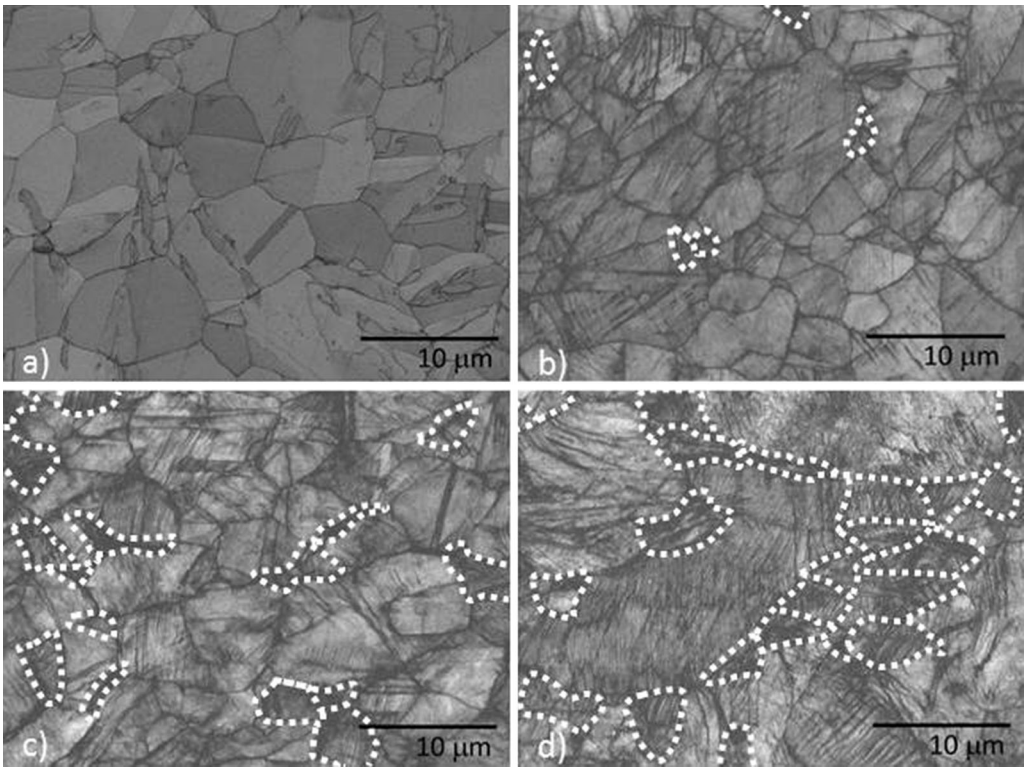


Fig. 4—Microstructure of the studied steel in annealed condition (*a*) and after cold rolling reductions of: (*b*) 10 pct, (*c*) 30 pct, and (*d*) 40 pct. Martensite phase identification by EBSD is enclosed in white dotted lines.

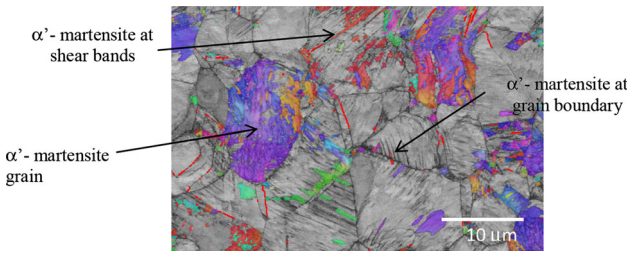


Fig. 5—EBSD orientation map of 20 pct cold-rolled sample (S2).

Small amounts of pre-existing martensite (9 ± 3 pct), led to a slight reduction on the average grain size, up to 8.8 ± 2.9 $\mu$m, compared to 3.8 ± 1.9 and 2.3 ± 1.5 $\mu$m achieved for martensite contents of 28 and 38 pct, respectively. In this regard, conventional industrial cold rolling process does not allow reducing grain size such as severe cold rolling and advanced thermo-mechanical process, where microstructure becomes ultrafine-grained (<100 nm) and even nanocrystallined (<50 nm).[8,10,13–15,17]

The wide grain size distribution observed for samples RS2 and RS3 (Figure 6) points out that austenite recrystallization takes place in various types of nucleation sites, as demonstrated by Rajasekhara *et al.*[10] This feature is typical of diffusion-type reversion mechanisms, in contrast with shear-type reversion mechanism where nucleation is time-independent and no austenite grain growth is observed.

## B. *Monotonic Mechanical Properties*

It is well known that mechanically induced martensite can enhance mechanical properties.[34–39] As demonstrated by the data in Figure 7, the higher the percentage of martensite, the higher the values of yield stress, ultimate strength, and hardness. It is important to point out that even for low amounts of pre-existing martensite, a relevant yield stress increase was observed. This becomes clear when yield stress values of AR and S1 samples are compared, the presence of 9 pct of pre-existing martensite leads to an increase from 360 to 650 MPa. On the other hand, the gap between yield stress and ultimate tensile strength becomes narrower as the cold rolling reduction rises, *i.e.*, the as-received steel condition displayed a ratio of 0.42 which increased up to 0.97 at cold reduction of 40 pct.

Significant discrepancy still exists in explaining the strengthening mechanisms of metastable austenitic stainless steels and, in concrete, the effect of the strain-induced $\alpha'$-martensite phase. Since the highly dislocated $\alpha'$-phase is much harder than the austenite, some authors[40,41] consider austenite-martensite mixtures as composites of soft austenitic matrix with hard martensite dispersion. Spencer *et al.*[42] demonstrated that martensite sustains a clearly higher stress than austenite, concluding that $\alpha'$-martensite acts as the reinforcing phase. In that sense, studies developed by Narutani *et al.*[43] for an AISI 301 steel concluded that for high martensite contents (>20 pct), the strengthening was related to the hardening

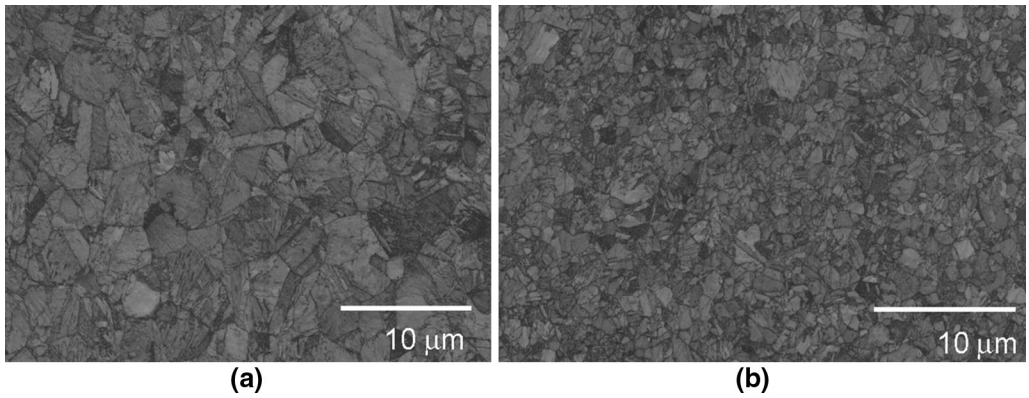


Fig. 6—Microstructure of (*a*) RS2 and (*b*) RS3 samples.

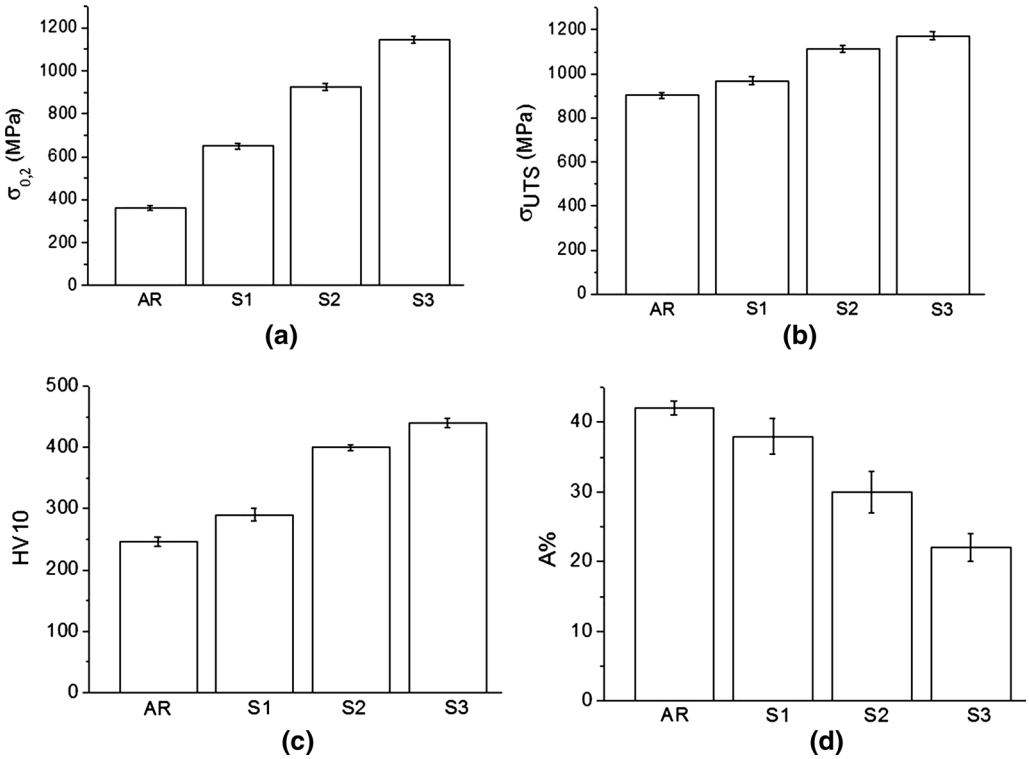


Fig. 7—Mechanical properties of steel after cold rolling: (*a*) yield strength, (*b*) ultimate strength, (*c*) hardness, and (*d*) ductility.

effect of the martensite by itself, while below this content, the formation of α′-martensite strengthens the steel by accelerating the dislocation generation in austenite. This effect was attributed to the accommodation of the volume expansion related to the transformation. Moreover, not only the influence of α′-martensite, but also the austenite strengthening, plays an important role on mechanical properties. As shown in Figure 8, nanoindentation measurements performed on austenitic grains revealed the effect of strain-hardening as increasing cold rolling reduction. The average hardness value displayed for the annealed condition (AR) was almost 50 pct lower than for cold-rolled sample S3.

Combined contribution of rising martensite transformation and austenite hardening causes a reduction of plastic deformation. As it can be observed in Figure 7(d), the ductility is inversely proportional to the initial amount of martensite. Numerous studies have focused on understanding the TRIP effect. The most widely accepted interpretation[44–47] is that not only the total amount of induced martensite is significant, but also the rate of transformation for a given plastic strain and at which point it takes place, are the factors that govern the ductility. The evolution of martensite transformation shown in Figure 9 demonstrates the validity of this interpretation. In this sense, for sample S2, whose

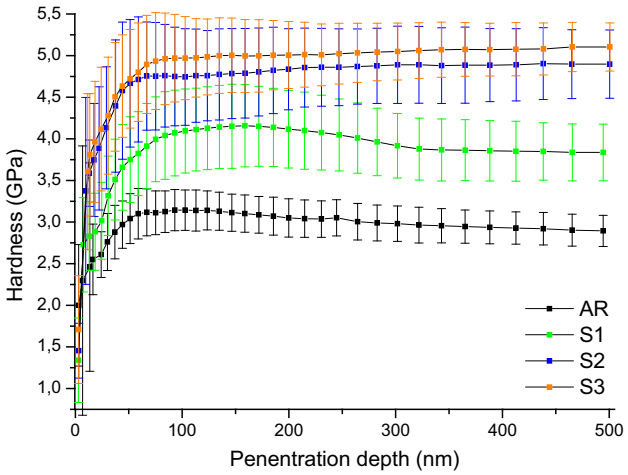


Fig. 8—Austenite hardness of the annealed (AR) and cold-rolled (S1, S2, S3) steel.

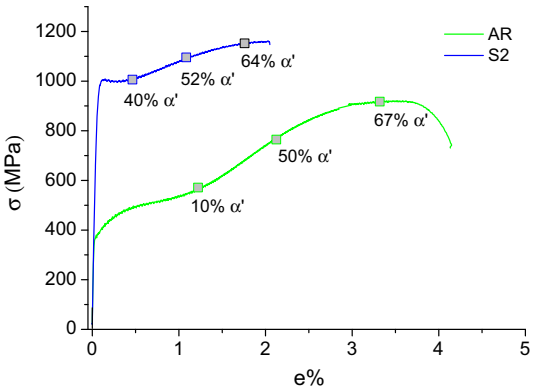


Fig. 9—Stress–strain curves for AR and S3 steel conditions indicating the percentage of α′-martensite at 30, 60, and 90 pct of their respective total elongation values.

initial martensite content was 28 pct, transformation occurs rapidly in comparison with AR, resulting in abrupt work hardening and, consequently, premature fracture.

Significant differences can be observed concerning fracture surfaces of tensile tested specimens. AR showed high density of dimples, generally associated with high plastic strain typical of ductile fracture (Figure 10(a)). For increasing pre-existing α′-martensite, fracture aspect is progressively shifting towards brittle (Figure 10(b) to (d)), with faceted areas and microcracks clearly distinguished. Assuming that the inclusions volume fraction is constant and at a very low level, the main embrittlement mechanisms are expected to be decohesioned at the austenite-martensite interface or separation of adjacent islands and localized deformation of martensite.

Figure 11 shows the effect of reversion treatments on the mechanical properties. It is important to point out that even small amount of pre-existing martensite (RS1) influences mechanical properties in such a way that yield strength achieves values higher than 40 pct comparing with untreated samples (AR) and with similar ductility. In this sense, it is clear that the smaller the grain size (corresponding to the steel conditions with high percentage of pre-existing martensite, RS2 and RS3) the higher the strength and the hardness. However, the ductility of the RS3 condition still displays at least 50 pct less ductility than AR samples. Detailed analysis of fracture surfaces reveals that, although RS3 presented large number of small dimples compared to AR (Figure 12), which it is known to increase ductility, microcracks and cracks randomly distributed on surface fracture were identified (Figure 13). These microcracks were also observed in cold-rolled samples S3. In this regard, it was assumed that contents of pre-existing martensite from cold rolling were still present in RS3 samples, *i.e.*, incomplete $\alpha' \rightarrow \gamma$ transformation phase took place during reversion treatments. Thus, for samples cold rolled at 40 pct thickness reduction (S3), it is necessary to apply higher temperatures or extend holding time to achieve fully austenitic microstructure.

It is well known that yield stress and hardness of a metallic material increase with decreasing grain size. In particular, the empirical Hall–Petch equation has been found to express this grain-size dependence.[48,49] Figure 14 clearly shows this inverse relationship, *i.e.*, both yield strength and hardness increase linearly when $d^{-1/2}$ goes from 11.7 $\mu$m, corresponding to the untreated steel (AR), up to 2.3 $\mu$m, value achieved after reversion treatments (RS3). These results are consistent and complement those shown by Huang *et al.*[28] which demonstrated that the Hall-Petch relationship for AISI 301LN held well down to 0.74 $\mu$m of mean austenitic grain size, while measurements on AISI 301 displayed deviation at about 3 $\mu$m grain size.[6]

## C. *Fatigue Tests*

Studies on the fatigue response of metastable stainless steels report different behaviors depending on the testing conditions.[50–54] The formation of martensite during deformation is known to be harmful in the low cycle fatigue regime, *i.e.*, under strain-control, while a small amount of martensite can be beneficial in the HCF regime.

A previous paper presented by the authors[55] demonstrated the possibility of improving the fatigue life of a metastable austenitic stainless steel by inducing martensitic transformation via torsion deformation previously to the HCF tests. In the present study, a similar trend was observed for cold-rolled samples S2 and S3. As shown in Table II, fatigue limits corresponding to those steel conditions are significantly higher in comparison with fully austenite microstructure (AR). After fatigue tests, X-ray diffraction patterns (Figure 15) revealed that α′-martensite increased up to 44 pct when the initial microstructure is fully austenitic (AR), while the amount created for the steel condition with a 28 pct of pre-existing martensite (S2) grew up 50 pct. As a result, significant differences were found regarding surface roughness associated with $\gamma \rightarrow \alpha'$ transformation, *i.e.*, $0.325 \pm 0.018$ $\mu$m and $0.198 \pm 0.021$ $\mu$m for AR and S2, respectively, compared with values lower than 0.1 $\mu$m before fatigue tests. These results are in

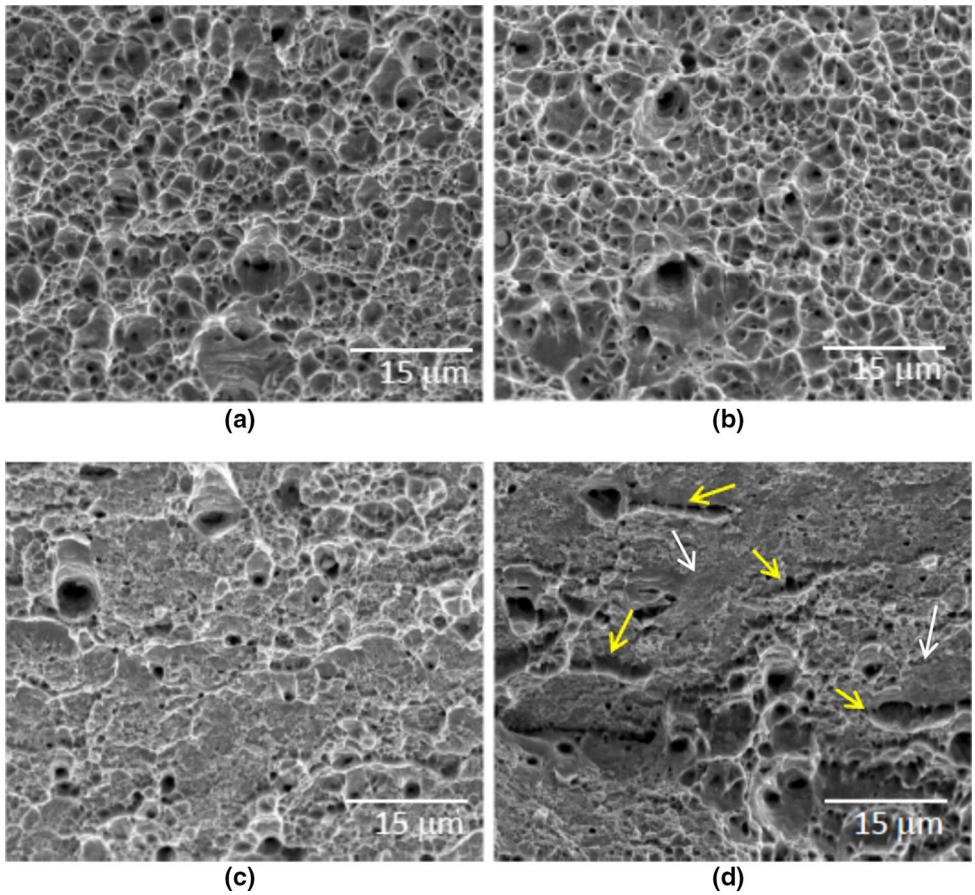


Fig. 10—SEM images of the fracture surfaces of tensile samples of: (*a*) AR, (*b*) S1, (*c*) S2, and (*d*) S3, yellow arrows indicate the presence of microcracks and white arrows point to faceted areas (Color figure online).

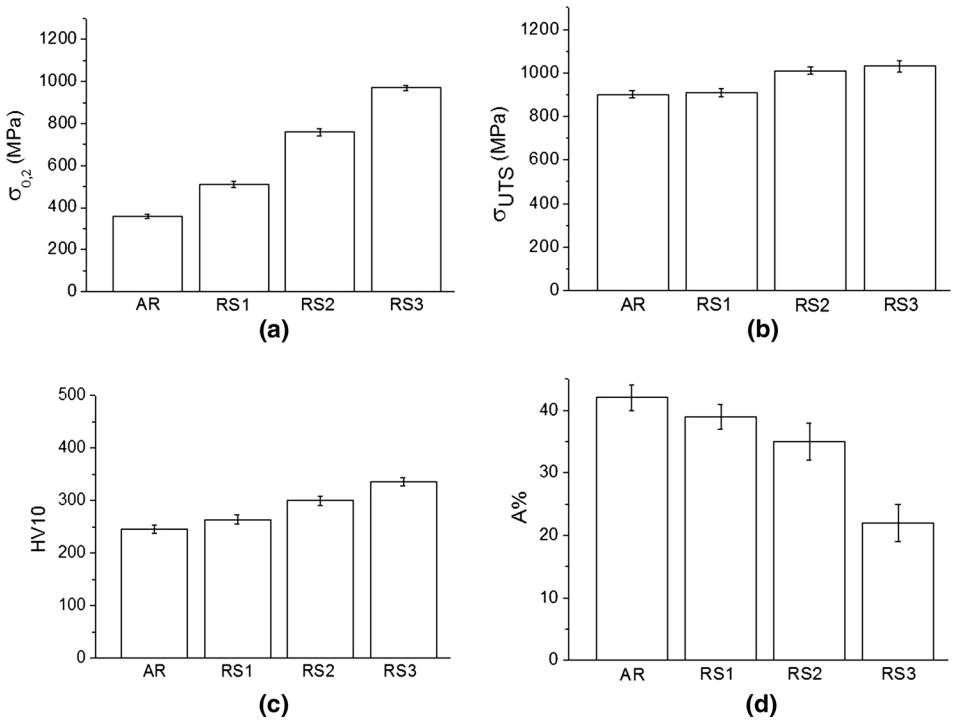


Fig. 11—Mechanical properties of steel after reversion: (*a*) yield strength, (*b*) ultimate strength, (*c*) hardness, and (*d*) ductility.

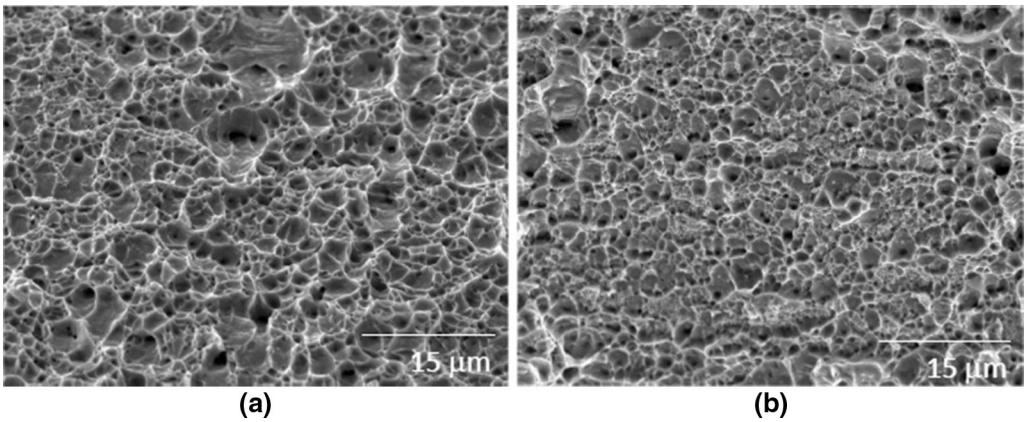


Fig. 12—SEM images of the fracture surfaces of tensile samples corresponding to: (*a*) Annealed steel, and (*b*) Reverted condition (RS3).

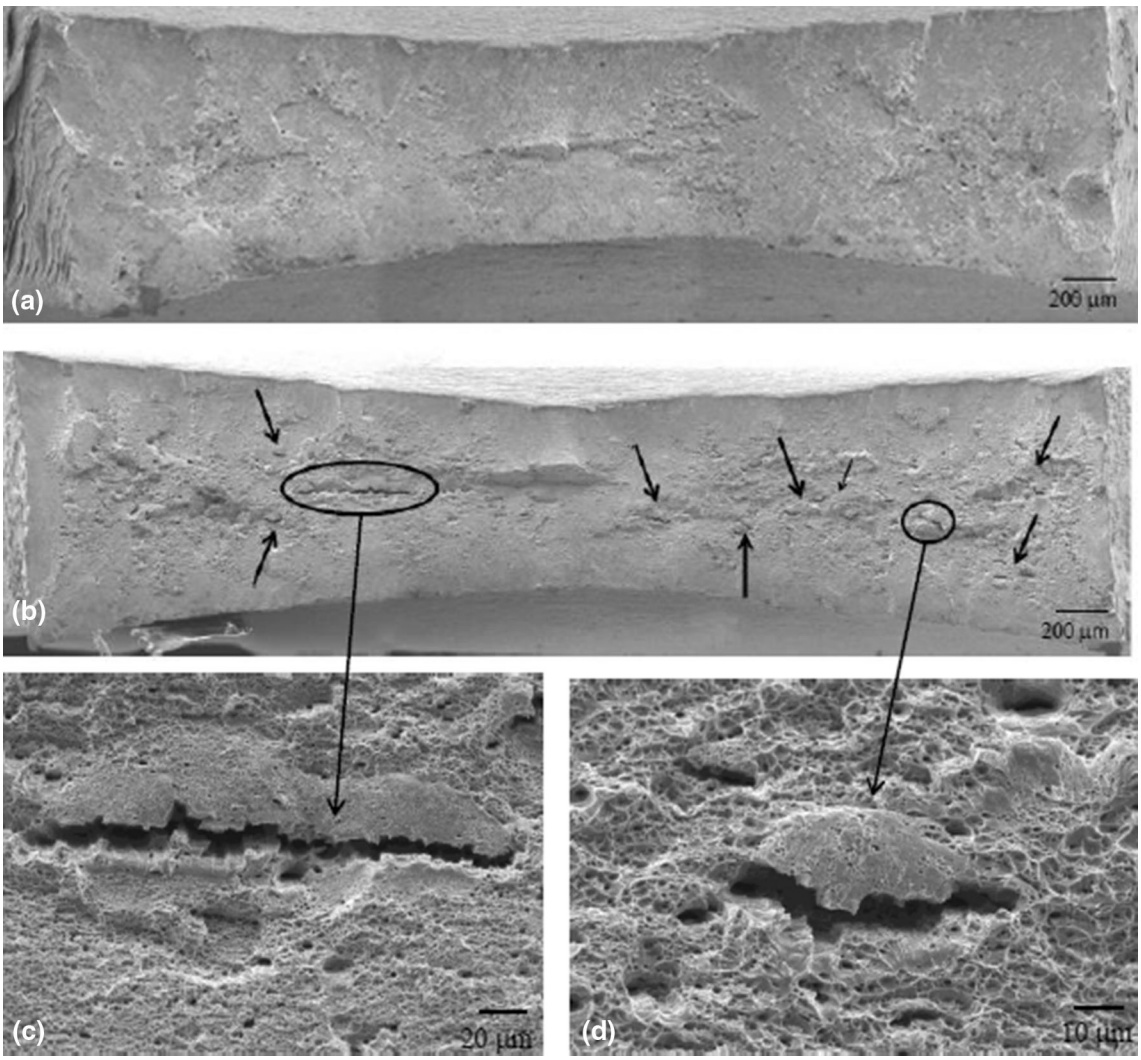


Fig. 13—SEM images of the fracture surfaces of tensile samples of: (*a*) Annealed steel (AR), and (*b*) Reverted condition (RS3), (*c*, *d*) Magnifications of cracks observed in figure b.

agreement with several studies which have pointed out that volume expansion associated with the martensitic transformation lead to the components distortion, dimensional changes, and even failure under extreme working conditions.[56,57] Moreover, authors demonstrated in a previous study carried out on the same steel grade,[58] that the amount of martensite formed during the first cycles of fatigue tests remains almost stable and martensite plates grow in height but neither in width nor in length. In this sense, it is assumed that higher roughness induces fatigue nucleation sites which dramatically influence fatigue behavior. In this regard, AR samples display higher "fatigue sensitivity" compared to S2 and S3. This parameter introduced by Fleck *et al.*,[59] is defined as the ratio between the maximum stress that the specimen is able to reach after $10^6$ cycles without fail and the ultimate tensile strength $[1 - (\sigma_{max}/\sigma_{UTS})]$. Fatigue sensitivity ranges from 0 to 1, so values closer to 0 indicate less sensitivity to fatigue. In that sense, results shown that at increasing percentage of pre-existing martensite, *i.e.*, S1 to S3, fatigue sensitivity progressively decreases becoming half of the value displayed for the fully austenitic steel (AR).

Grain size refinement achieved by reversion treatments led to fatigue limits clearly higher than the value corresponding to AR condition, Table III. This effect was more pronounced for samples RS2 and RS3, but even for the steel condition with the lowest percentage of pre-existing $\alpha'$-martensite (RS1) an increase of 12 pct on fatigue limit was measured. This is consistent and

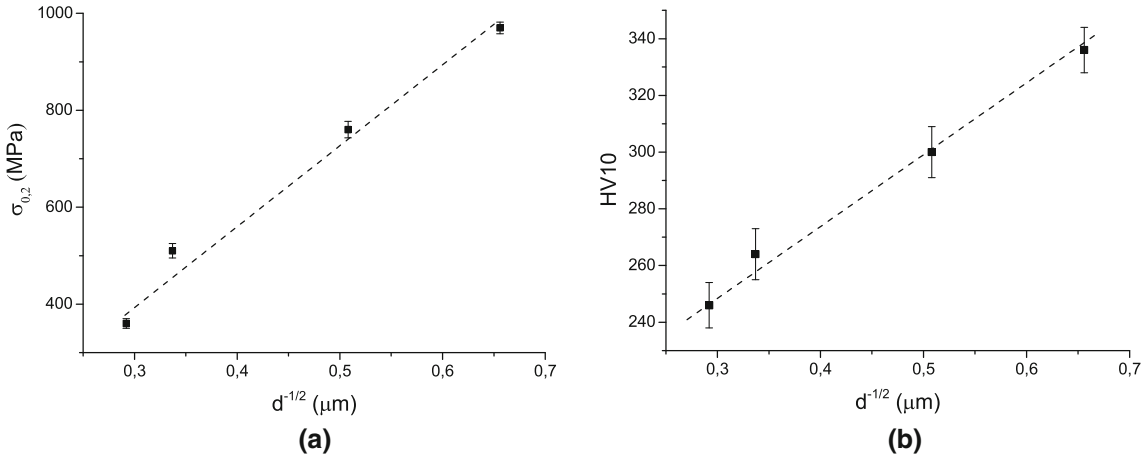


Fig. 14—Dependence of the grain size on: (*a*) yield strength and (*b*) hardness.

**Table II. Fatigue Limit and Fatigue Sensitivity for Studied Steel Conditions**

| Steel Conditions | AR | S1 | S2 | S3 |
|---|---|---|---|---|
| $\sigma_{max}$ (MPa) | 570 ± 56 | 680 ± 49 | 895 ± 71 | 956 ± 88 |
| Fatigue sensitivity | 0.37 | 0.30 | 0.20 | 0.18 |

**Table III. Fatigue Limit and Fatigue Sensitivity After Reversion Treatments**

| Steel Conditions | AR | RS1 | RS2 | RS3 |
|---|---|---|---|---|
| $\sigma_{max}$ (MPa) | 570 ± 56 | 640 ± 44 | 795 ± 58 | 880 ± 43 |
| $1 - (\sigma_{max}/\sigma_{UTS})$ | 0.37 | 0.30 | 0.22 | 0.15 |

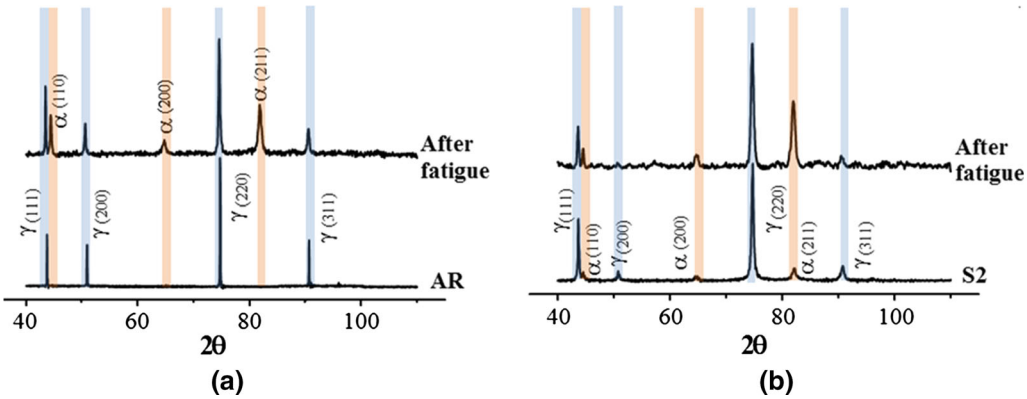


Fig. 15—X-ray diffraction patterns of the annealed (AR) and cold-rolled (S2) samples after $10^6$ fatigue cycles.

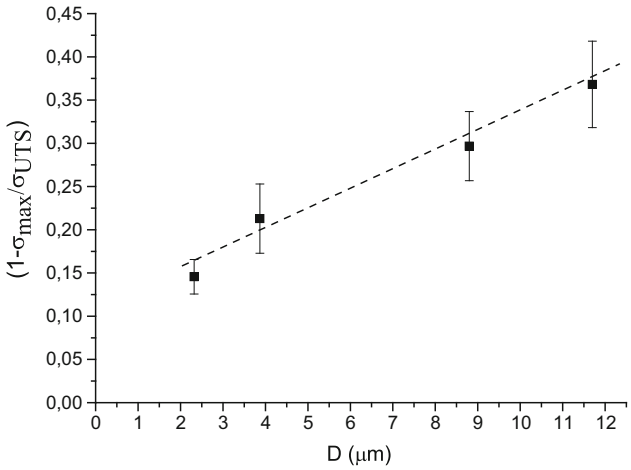


Fig. 16—Effect of grain size on fatigue sensitivity.

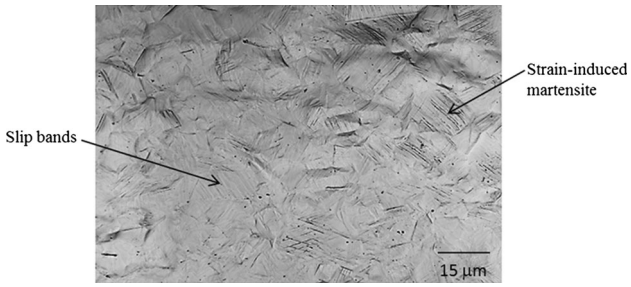


Fig. 17—Slip bands and strain-induced martensite after fatigue tests on annealed steel (AR).

complements earlier investigations[16,60] carried on reverted AISI 301LN steel with higher percentages of pre-existing $\alpha'$-martensite (>80 pct) than those studied in this work. It was also observed that $\gamma \rightarrow \alpha'$ phase transformation was significantly reduced at decreasing grain size. After fatigue tests, the amount of strain-induced martensite was close to 44 pct for the AR, while reverted samples (RS3) showed values not higher than 23 pct. As some authors have demonstrated,[61–63] basically two reasons can explain this behavior: the higher strength of fine-grained austenite which slows up the strain-induced martensite formation and the increasing of SFE due to grain refinement, taking into account that higher SFE means higher austenite stability.

Another important feature achieved by reverted austenite microstructure is the progressive reduction of fatigue sensitivity as grain size decreases (Figure 16). SEM analysis performed in plain view areas close to the fracture surface revealed the formation of intensive slip bands crossing the grains for the condition with bigger grain size (AR), Figure 17, compared to RS3 samples where less density of slip bands was observed. This trait, even observed for ultrafine-grained and nanocrystalline microstructures,[15,16] together with lower fatigue-induced martensite content at the samples surface and its corresponding volume expansion (as much as 4 pct)[64–66] was assumed to be critical to reduce crack nucleation sites and as a consequence fatigue sensitivity.

## IV. CONCLUSIONS

The effect on microstructural characteristics and mechanical properties, both monotonic and cyclic, of the martensite induced by industrial cold rolling processes, with a thickness reduction up to 40 pct, was analyzed. Moreover, the influence of reversion heat treatments, that remove martensite and lead to a smaller austenitic grain size, was studied too. The following conclusions can be extracted concerning the influence of strain-induced martensite:

– No evidence of $\varepsilon$-martensite was detected on the studied cold-rolled samples. The formation of $\alpha'$-martensite develops mainly at shear bands and increases progressively with the cold rolling reduction, but not linearly.
– Small amounts of $\alpha'$-martensite, formed after 10 pct of cold rolling, increase more than 50 pct the yield stress, as compared with AR, whereas after 40 pct of cold working yield stress triplicates the initial one.
– Cold rolling has a positive effect on the fatigue limit too. $\alpha'$-martensite formed by 10-pct cold rolling enhanced fatigue limit around 20 pct compared to AR. Higher cold working levels allowed values 60 pct higher.

With regard to the effect of reversion treatments, it can be stated that:

– Reversion treatments demonstrated to be a feasible way to obtain grain refinement, simultaneously avoiding the presence of martensite. The average austenitic grain size decreased by 25 pct for samples with 10 pct of cold working reduction, whereas 80 pct of grain refinement was reached after 40 pct of cold rolling.
– Hall-Petch relationship between austenite grain size, yield strength, and hardness works well for reversed microstructures ranging from 0.29 to 0.66 $\mu$m.
– Even for small amounts (less than 10 pct) of pre-existing martensite reversion treatments provided a significant increment (40 pct) on yield stress over the AR.
– Upon reversion, enhanced fatigue limit, as compared to AR, was measured for specimens previously subjected to 20 pct and 40 pct of cold rolling reduction. On the other hand, less intensively rolled samples (only 10 pct of reduction) did not display a higher fatigue limit.

## ACKNOWLEDGMENTS

The present work was carried out within the scope of MAT09-14461 project, supported by the Spanish Ministry of Economy. We are grateful to "*Direcció General de Recerca del Comissionat per a Universitats i Recerca de la Generalitat de Catalunya*" for recognizing CIEFMA as a consolidated Research Group (2009SGR). Dr. J. J. Roa would like to thank Juan de

la Cierva Programme (Grant Number JCI-2012-14454) for its financial support.

## REFERENCES


1. F. Placidi and F. Fraschetti: *Potential application of stainless steel for vehicle crashworthiness structures*. Technical report, Cenro sviluppo materiali, Italy.
2. A. Di Schino, J.M. Kenny, M.G. Mecozzi, and M. Barteri: *J. Mater. Sci.*, 2000, vol. 35, pp. 4803–08.
3. T. Christiansen and M.A.J. Somers: *Metal. Mater. Trans. A*, 2006, vol. 37A, pp. 675–82.
4. S.S. Hecker, M.G. Stout, and J.L. Smith: *Metall. Trans.*, 1982, vol. 13A, pp. 619–26.
5. H.F.G. de Abreu, M.J.G. da Silva, L.F.G. Herculano, and H. Bhadeshia: *Mater. Res.*, 2009, vol. 12, pp. 291–97.
6. A. Di Schino, M. Barteri, and J.M. Kenny: *J. Mater. Sci. Lett.*, 2002, vol. 21, pp. 751–53.
7. J.Y. Choi and W. Jin: *Scr. Mater.*, 1997, vol. 36, pp. 99–104.
8. M. Karimi, A. Najafizadeh, A. Kermanpur, and M. Eskandari: *Mater. Charact.*, 2009, vol. 60, pp. 1220–23.
9. M.C. Somani, L.P. Karjalainen, A. Kyröläinen, and T. Taulavuori: *Mater. Sci. Forum*, 2007, vols. 539–543, pp. 4875–7880.
10. S. Rajasekhara, L.P. Karjalainen, A. Kyröläinen, and P.J. Ferreira: *Mater. Sci. Eng. A*, 2010, vol. 527, pp. 1986–96.
11. A. Di Schino and J.M. Kenny: *Mater. Lett.*, 2003, vol. 57, pp. 3182–85.
12. A.S. Hamada, L.P. Karjalainen, and M.C. Somani: *Mater. Sci. Eng. A*, 2006, vol. 431, pp. 211–17.
13. R.D.K. Misra, B. Ravi Kumar, M. Somani, and P. Karjalainen: *Scr. Mater.*, 2008, vol. 59, pp. 79–82.
14. M.C. Somani, P. Juntunen, L.P. Karjalainen, R.D.K. Misra, and A. Kyröläinen: *Metall. Mater. Trans. A*, 2009, vol. 40A, pp. 729–44.
15. A.S. Hamada, L.P Karjalainen, P.K.C. Venkata v, and R.D.K. Misra: *Mater. Sci. Eng. A*, 2011, vol. 528, pp. 3890–96.
16. A. Järvenpää, L. Pentti Karjalainen, and M. Jaskari: . *Int. J. Fatigue*, 2013, vol. 65, pp. 93–98.
17. J. Huang, X. Ye, J. Gu, X. Chen, and Z. Xu: *Mater. Sci. Eng. A*, 2012, vol. 532, pp. 190–95.
18. O.V. Mishin, D.J. Jensen, and N. Hansen: *Mater. Sci. Eng. A*, 2003, vol. 342, pp. 320–28.
19. T.S. Wang, J.G. Peng, Y.W. Gao, F.C. Zhang, and T.F. Jing: *Mater. Sci. Eng. A*, 2005, vol. 407, pp. 84–88.
20. A. Mateo, A. Hernández, A. Zapata, P. Rodríguez-Calvillo, G. Fargas, J. Calvo, and D. Casellas: *XII Congreso Iberoamericano de Materiales IBEROMAT XII*, Univ. Alicante A-20, 2012.
21. ASTM E975-03: *Standard Practice for X-Ray Determination of Retained Austenite in Steel with Near Random Crystallographic Orientation*, ASTM International, West Conshohocken, 2003.
22. W.C. Oliver and G.M. Pharr: *J. Mater. Res.*, 1992, vol. 7, pp. 1564–83.
23. W.C. Oliver and G.M. Pharr: *J. Mater. Res.*, 2004, vol. 19, pp. 3–20.
24. ASTM E 8-04: *Standard Test Methods for Tension Testing of Metallic Materials*, 2008.
25. A.M. Mood and W.J. Dixon: *J. Am. Stat. Assoc.*, 1948, vol. 43 (241), pp. 109–126.
26. D. Grove and F. Campean: *Test*, 2008, vol. 24, pp. 485–97.
27. A. Mateo, G. Fargas, J.J. Roa, and J. Calvo: *Mater. Test.*, 2015, vol. 57, pp. 2–5.
28. J.X. Huang, X.N. Ye, and Z. Xu: *J. Iron Steel Res. Int.*, 2012, vol. 19 (10), pp. 59–63.
29. J. Talonen, P. Aspengen, and H. Hänninen: *Mater. Sci. Technol.*, 2004, vol. 20 (12), pp. 1506–512.
30. A.M. Beese and D. Mohr: *Exp. Mech.*, 2011, vol. 51, pp. 667–76.
31. R.E. Schramm and R.P. Reed: *Metall. Trans.*, 1975, vol. 6A, pp. 1345–51.
32. A.F. Padilha, R.L. Plaut, and P.R. Rios: *ISIJ Int.*, 2003, vol. 43 (2), pp. 135–43.
33. J.J. Roa, G. Fargas, J. Calvo, E. Jiménez-Piqué, and A. Mateo: *Mater. Sci. Eng. A.*, 2015, vol. 628, pp. 410–18.
34. F. Lecroisey and A. Pineau: *Metall. Trans.*, 1972, vol. 3, pp. 387–96.
35. G.D. Huang, D.K. Matlock, and G. Krauss: *Metall. Trans. A*, 1989, vol. 20 (7), pp. 1239–46.
36. X.F. Fang and W. Dahl: *Mater. Sci. Eng. A*, 1991, vol. 141 (2), pp. 189–98.
37. T.S. Byun: *Acta Mater.*, 2003, vol. 51 (11), pp. 3063–3071.
38. J. Talonen, P. Nenonen, G. Pape, and H. Hanninen: *Met. Mater. Trans. A*, 2005, vol. 36 (2), pp. 421–32.
39. A.M. Beese and D. Mohr: *J. Mech. Phys. Solids*, 2012, vol. 60 (11), pp. 1922–40.
40. P.L. Mangonon and G. Thomas: *Metall. Trans.*, 1970, vol. 1 (6), pp. 1587–94.
41. I. Tamura: *Metal Sci.*, 1982, vol. 16 (5), pp. 245–53.
42. K. Spencer, J.D. Embury, K.T. Conlon, M. Véron, and Y. Bréchet: *Mater. Sci. Eng. A*, 2004, vols. 387–389, pp. 873–81.
43. T. Narutani: *Mater. Trans. JIM*, 1989, vol. 30 (1), pp. 33–45.
44. G.P. Sanderson and D.T. Llewellyn: *J. Iron Steel Ins.*, 1969, vol. 207 (8), pp. 1129–40.
45. A. Rosen, R. Jago, and T. Kjer: *J. Mater. Sci.*, 1972, vol. 7 (8), pp. 870–76.
46. N. Tsuchida and Y. Tomota: *Mater. Sci. Eng. A*, 2000, vol. 285 (1-2), pp. 345–52.
47. Y. Tomota, H. Tokuda, Y. Adachi, M. Wakita, N. Minakawa, A. Moriai, and Y. Morii: *Acta Mater.*, 2004, vol. 52 (20), pp. 5737–45.
48. J.N. Petch: *J. Iron Steel Inst.*, 1953, vol. 174, pp. 25–28.
49. E.O. Hall: *Proc. Phys. Soc.*, 1951, vol. 64B, pp. 747–53.
50. G.R. Chanani, S.D. Antolovich, and W.W. Gerberich: *Metall. Trans.*, 1972, vol. 3, pp. 2661–72.
51. G. Baudry and A. Pineau: *Mater. Sci. Eng.*, 1977, vol. 28, pp. 229–42.
52. C. Bathias and R.M. Pelloux: *Metall. Mater. Trans. B*, 1973, vol. 4B, pp. 1265–73.
53. J. Stolarz, N. Baffie, and T. Magnin: *Mater. Sci. Eng. A*, 2001, vols. 319–321, pp. 521–26.
54. M. Topic, R.B. Tait, and C. Allen: *Int. J. Fatigue*, 2007, vol. 29, pp. 656–65.
55. G. Fargas, A. Zapata, M. Anglada, and A. Mateo: *IOP Conf. Ser. Mater. Sci. Eng.*, 2009, vol. 5, p. 012008.
56. D. Mohan Lal, S. Renganarayanan, and A. Kalanidhi: *Cryogenics*, 2001, vol. 4, pp. 149–55.
57. D. Das, K.K. Ray, and A.K. Dutta: *Mater. Sci. Eng. A*, 2010, vol. 527, pp. 2182–93.
58. J.J. Roa, G. Fargas, E. Jiménez-Piqué, and A. Mateo: *Mater. Sci. And Eng. A*, 2014, vol. 597, pp. 232–36.
59. N.A. Fleck, K.J. Kang, and F. Ashby: *Acta Metall. Mater.*, 1994, vol. 42, pp. 365–81.
60. A.S. Hamada and L.P. Karjalainen: *Mater. Sci. Eng. A*, 2010, vol. 527, pp. 5715–22.
61. J.E. Jin, Y.S. Jung, and Y.K. Lee: *Mater. Sci. Eng. A*, 2007, vols. 449–451, pp. 786–89.
62. J.H. Jun and C.S. Choi: *Mater. Sci. Eng. A*, 1998, vol. 257, pp. 353–56.
63. R.D.K. Misra, Z. Zhang, Z. Jia, M.C. Somani, and L.P. Karjalainen: *Scr. Mater.*, 2010, vol. 63, pp. 1057–60.
64. Y.D. Wang, R.L. Peng, and R.L. McGreenvya: *Acta Mater.*, 2002, vol. 50, pp. 1717–34.
65. A. Bahadur, B.R. Kumar, and S.G. Chowdhury: *Mater. Sci. Technol.*, 2004, vol. 20, pp. 387–92.
66. T.V. Rajan, C.P. Sharma, and A. Sharma: *Heat treatment: Principles and Techniques*, 2 Eastern Economy Ednd ed., East West Academic Books LLC, Burlington, 2011, p. 200.